Journal of Ceramic Science and Technology

Zirconia-Mullite Obtained from Co-Precipitated Zirconia-Mullite Composite Powders by SPS

H.Z. Li[1], Z.J. Li[1], X.D. Luo[*1], J.Y. Gui[2], Z.P. Xie[2]

[1]School of High Temperature Materials and Magnesium Resource Engineering,
University of Science and Technology Liaoning, Anshan 114051, China
[2]State Key Laboratory of New Ceramics and Fine Processing, School of Materials
Science and Engineering, Tsinghua University, Beijing 100084, China

Abstract

The co-precipitation method is used to fabricate precursor powder. This powder is densified by means of the spark plasma sintering (SPS) technique at 1500 °C with a holding time of 7 min to prepare zirconia-mullite samples. Their density measures up to 97 % of the theoretical density, and the sintered mullite compacts exhibit better strength properties (289 ± 12 MPa) and H_v (9.99 GPa). The mode of fracture is changed with the addition of ZrO_2 and extensive fine cleavages are observed on the grain surface. These cleavages join together to form steps, which can absorb more energy. The flexural strength of the samples is almost double that of pure mullite, which is related to the formation of cleavages.

Keywords: Zirconia-mullite, co-precipitation, flexural strength, Vickers hardness, microstructure

I. Introduction

Owing to its high refractoriness, chemical resistance, high creep resistance, thermal shock resistance and attractive bending strength at high temperatures, mullite has received significant attention during the last decades, and consequently it has been widely used in a great number of engineering fields [1–4]. However, mullite by itself suffers from low mechanical properties at room temperature [5]. Mullite is a solid solution compound $(Al_2[Al_{2+2x}Si_{2-2x}]O_{10-x}, 0.18≤x≤0.82)$, which is the sole stable phase in the Al_2O_3-SiO_2 system [6]. Its structure can be described as edges-shared $[AlO_6]$ octahedron chains parallel to a c-axis bounded by aluminium and/or silicon tetrahedra [7]. Usually, it is very difficult to obtain mullite with high density by means of traditional techniques (ball-milling, pressureless sintering) owing to the low diffusivities of aluminium and silicon within the mullite lattice. Also, the conventional solid-state reaction process for synthesizing mullite powders requires an extremely high temperature [8]. Recently, chemical process approaches have been applied to prepare mullite powders; of these approaches the co-precipitation method is the most common. For instance, mullite was formed at ~ 1000 °C in a molecularly mixed amorphous single system [9].

The formation of mullite was related not only to material processing but also to the introduction of other compounds, especially oxides. For example, introducing Y_2O_3, La_2O_3, CeO_2 into Al_2O_3/SiO_2 mixtures signifi-cantly lowers the mullitization temperature owing to the formation of low-viscosity liquid phase [10]. The addition of B_2O_3 can also lower the mullitization temperature, which is attributed to the fact that B_2O_3 dramatically reduces the viscosity of the SiO_2-rich liquid phase and reacts with alumina to form an aluminum borate compound ($9Al_2O_3$ ·$2B_2O_3$) acting as nuclei for the crystallization of mullite [11]. Moreover, MgO has been incorporated into fly-ash/bauxite mixtures to promote their densification by forming a magnesia-containing silica-rich ternary liquid phase [12]. Introducing ZrO_2 as reinforcement in the mullite matrix can enhance the mechanical properties of mullite. A series of ceramic composites from the Al_2O_3-SiO_2-ZrO_2 system have been reported. And some advanced sintering techniques such as hot pressing, microwave sintering, spark plasma sintering (SPS) and so on have been used to obtain high-performance mullite ceramics [13–14]. SPS is an excellent technique to densify any class of materials, especially materials that are difficult to sinter with conventional techniques. A complete description of the SPS technique can be found elsewhere [15–17]. However, few people have studied the doping method (chemical method) and adopted SPS to fabricate zirconia-mullite.

In this study, we have described the effects of zirconia, which is doped by means of the chemical method. The effects of the calcination temperature on the precursor powders have been discussed. The microstructure and mechanical properties have also been investigated.

* Corresponding author: luoxudongs@aliyun.com

II. Experimental Procedure

(1) Powder preparation

The precursor powders applied in this study were obtained using the co-precipitation method. For the mullite precursor powders (labeled 0#), aluminum sulfate ($Al_2(SO_4)_3 \cdot 18H_2O$) and sodium silicate ($Na_2SiO_3 \cdot 9H_2O$) were used as raw materials. With regard to the mullite precursor powders containing ZrO_2, $ZrCl_4$ was incorporated from 1 to 4 wt% during the preparing process, and the corresponding precursor powders were designated 1#, 2#, 3# and 4#, respectively. Their specific preparation method was as follows: the sodium silicate was first dissolved in the deionized water, and then hydrochloric acid was added to obtain a silica sol by refluxing for 20 min. Subsequently, the aluminum sulfate solution and ammonia were added to prepare aluminum hydroxide precipitation. After that, the mixture was refluxed for 15 min and aged for 20 min. The precipitate was filtered and azeotropically distilled using a rotary evaporator to prepare the precursor powders. A schematic illustration of the co-precipitation method is shown in Fig. 1. The precursor powders were treated at 400 – 1000 °C for 0.5 h at the rate of 10 K/min.
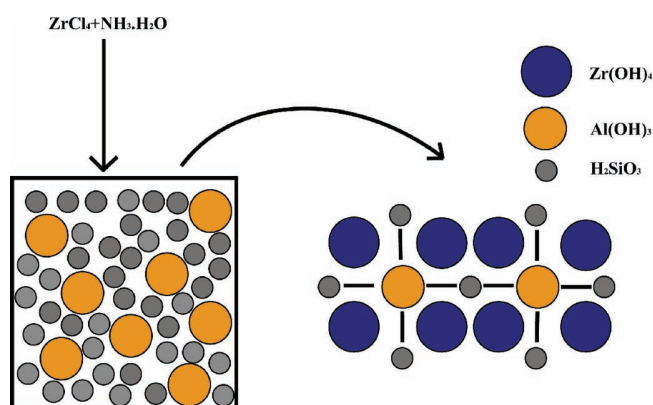

Fig. 1: A schematic illustration of the co-precipitation method.

The precursor powders applied in this study were obtained using the co-precipitation method. For the mullite precursor powders (labeled 0#), aluminum sulfate ($Al_2(SO_4)_3 \cdot 18H_2O$) and sodium silicate ($Na_2SiO_3 \cdot 9H_2O$) were used as raw materials. With regard to the mullite precursor powders containing ZrO_2, $ZrCl_4$ was incorporated from 1 to 4 wt% during the preparing process, and the corresponding precursor powders were designated 1#, 2#, 3# and 4#, respectively. Their specific preparation method was as follows: the sodium silicate was first dissolved in the deionized water, and then hydrochloric acid was added to obtain a silica sol by refluxing for 20 min. Subsequently, the aluminum sulfate solution and ammonia were added to prepare aluminum hydroxide precipitation. After that, the mixture was refluxed for 15 min and aged for 20 min. The precipitate was filtered and azeotropically distilled using a rotary evaporator to prepare the precursor powders. A schematic illustration of the co-precipitation method is shown in Fig. 1. The precursor powders were treated at 400 – 1000 °C for 0.5 h at the rate of 10 K/min.

(2) Sample preparation

The dried mixtures were sieved through a 100-mesh and then 7.5 g as-prepared powder was placed into a graphite die (30 mm in diameter) lined with graphite sheets to avoid a reaction between the powders and the die during the sintering process. The samples were sintered with the Dr. Sinter SPS-1050T spark plasma sintering system (SPS, Sumitomo Coal Mining Co. Ltd., Japan) in vacuum, and an infrared thermometer was used to measure the temperature. The powder was heated from room temperature up to 600 °C for 4 min, and subsequently up to the sintering temperature of 1500 °C with ~ 100 K min^{-1} heating rate and 7 min holding time. The applied uniaxial pressure was 50 MPa and maintained for 7 min at the final sintering temperature.

(3) Testing and characterization

Differential scanning calorimeter (DSC) analysis (STA 409 PC/PG, Netzsch, Germany) was performed in air at a heating rate of 10 K/min. Also, x-ray diffraction analysis (D8ADVANCE A25, Bruker, Germany) was performed at 40 kV and 40 mA using graphite monochromatic Cu Kα radiation at a range of 2θ from 10 ° to 90 °, with a step size of 0.02 °and a rate of 6 °/min. The Archimedes technique was used to measure the density of the SPS-sintered samples (METTLER TOLEDO ME204, METTLER, Switzerland). The relative density of the SPS-sintered samples was calculated according to the following relation (Eq. 1):

$$\rho_{Rel} = \rho_{Measured}/\rho_{Theory} \tag{1}$$

where ϱ_{Rel} is the relative density, $\varrho_{Measured}$ is the measured density and ϱ_{Theory} is the theoretical density. The theoretical density of the reaction-sintered samples can be determined from the weight percentage of different phases according to the following equation (Eq. 2):

$$\rho_{Theory} = 100/(X_A/\rho_A + X_B/\rho_B) \tag{2}$$

where X_i is the weight percentage of phase i and ϱ_i is its density (g/cm^3) [5].

The microstructure of the specimens was characterized using scanning electron microscopy (SEM) (Zeiss ΣIGMA HD). Flexural strength was measured by means of the three-point bending method in a universal testing machine (AG-IC; Shimadzu, Kyoto, Japan) on 1.5 mm × 2 mm × 15 mm specimens with a loading speed of 0.5 mm/min. Between 7 and 10 specimens were used for a data point for flexural strength. The Vickers hardness (H_v) was measured with a Vickers indentation machine (Wilson Vivtorinox Tukon 2500, USA). At least seven indentions under 1 kg load for each sample were performed [2, 18 – 19]. The fracture toughness (K_{IC}) was calculated according to the following equation (Eq. 3):

$$K_{IC} = 0.016 \cdot (P/C_0^{3/2})(E/H)^{1/2} \tag{3}$$

where E is the modulus of elasticity, H is the Vickers hardness, P is the indentation test load, c is the indentation crack length. The crack lengths were measured immediately after the indentation in order to avoid slow crack growth after the load was removed. The E value employed was 240 GPa.

III. Results and Discussions

(1) TG-DSC and XRD

Fig. 2(a) shows the TG-DSC curve of the mullite precursor. A unique sharp exothermic peak occurs at ~ 1000 °C. Also, a very small exothermic peak can be perceptible at ~ 1300 °C, which is consistently recognized as the sign of reaction between the formed spinel and amorphous silica. Fig. 2(b) shows XRD patterns of the precursor powders treated at different temperatures. It can be found that the precursor powders dried at 110 °C are in the amorphous state and retain this state until 1000 °C. The result is in good agreement with the TG-DSC analysis.
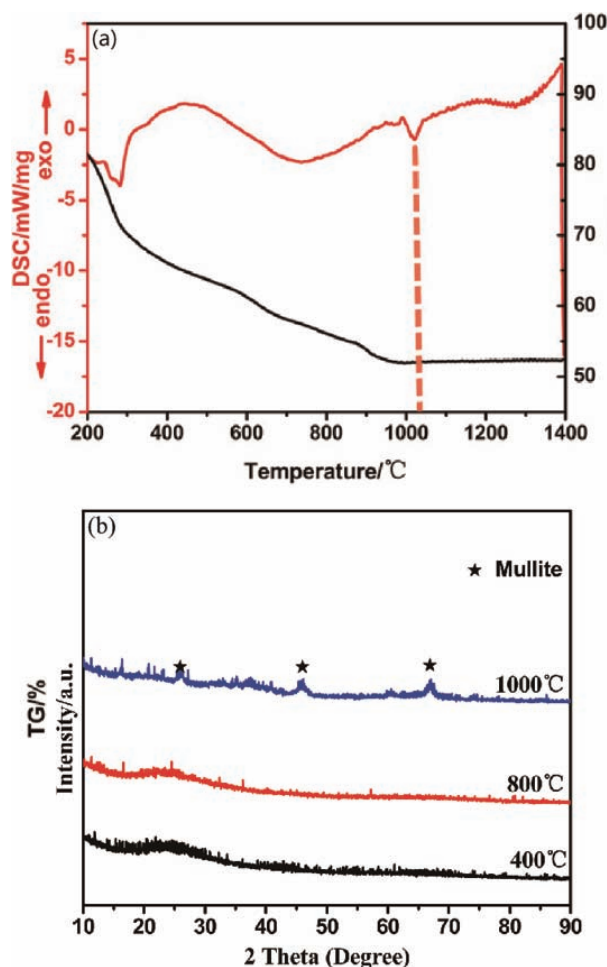

Fig. 2: (a) The TG-DSC curve of the mullite precursor powders; (b) XRD patterns of the precursor powders treated at different temperatures.

(2) Density and Vickers hardness

Fig. 3 shows the relative density and Vickers hardness of sintered mullite ceramics doped with ZrO_2. Nearly full densification (> 97 % of theoretical density) is successfully achieved by means of SPS with up to 2.0 wt% ZrO_2 addition, which is consistent with the dense microstructures. However, the relative density gradually decreases as the ZrO_2 content increases, indicating that ZrO_2 impedes the densification of the ceramics. Because of the difference of the cation size, ZrO_2 segregates above 2.0 wt% excess. This is probably the reason why the material does not densify properly.

The Vickers hardness firstly increased from 7.17 GPa to 9.99 GPa with a small amount of ZrO_2 (2.0 wt%) added, and then decreased to 8.06 GPa with the further addition of ZrO_2 (4.0 wt%), as shown in Fig. 3. The result signifies that the Vickers hardness of this composite material is strongly dependent on its density. Hence 2.0 wt% is adopted as the optimal content in the following discussion.
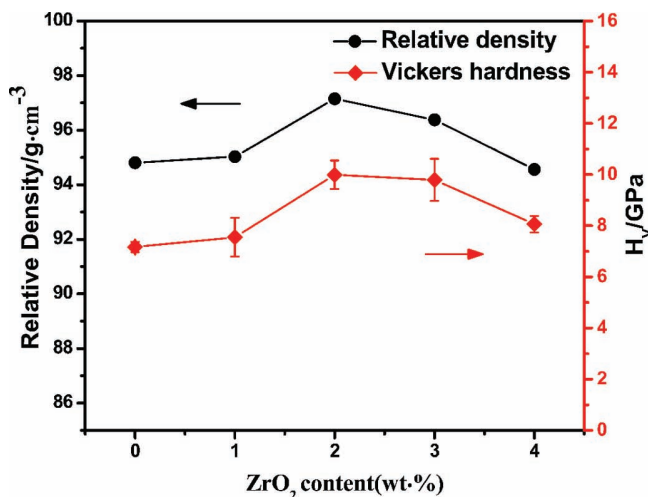

Fig. 3: The relative density and Vickers hardness of ZrO_2-mullite ceramics.

(3) Microstructure

The fracture surface morphology of mullite ceramics toughened by ZrO_2 is shown in Fig. 4. The mullite ceramic exhibits a dense microstructure and the fracture mode is changed by introducing ZrO_2 (Figs. 4(a)-4(c)). The growth of rod-like particles in the ZrO_2-mullite ceramics changed the fracture mode from mainly transgranular to the mixed type of intergranular and transgranular. A lower magnification micrograph showed predominantly transgranular mode of fracture, and the fracture along the grain boundaries also occurred in some places (see the insert Fig. 4(d)). On experiencing a grain boundary fracture, the area of fracture increased and it was able to absorb much more energy[20]. Therefore, the growth of rod-like mullite would increase the fracture surface energy of mullite ceramics.

Also, some cleavages were observed in the ZrO_2-mullite ceramics. An example of this is shown in Figs. 4(b) and 4(c). Grain A has extensively cleaved morphologies, and the regions B and C in other grains show some cleavages. A pore (D) will be left when a grain is pulled out. An intracrystalline pore (E) exists in Fig. 4(c). Fig. 4(d) is an enlarged area, in which the morphology of the mullite grain is elongated and columnar, and the average particle diameter is 600 nm. Fig. 4(e) is a schematic illustration of fracture mode in the cleavage plane. When the crack went through the contorted grain boundaries and expanded from grain ① into grain ②, grain ② was split into several segments at the leading edge area in the process of crack's expansion. The crack extended from the tip to the bottom, forming a 'river pattern' fracture mode[21]. The presence of pores and
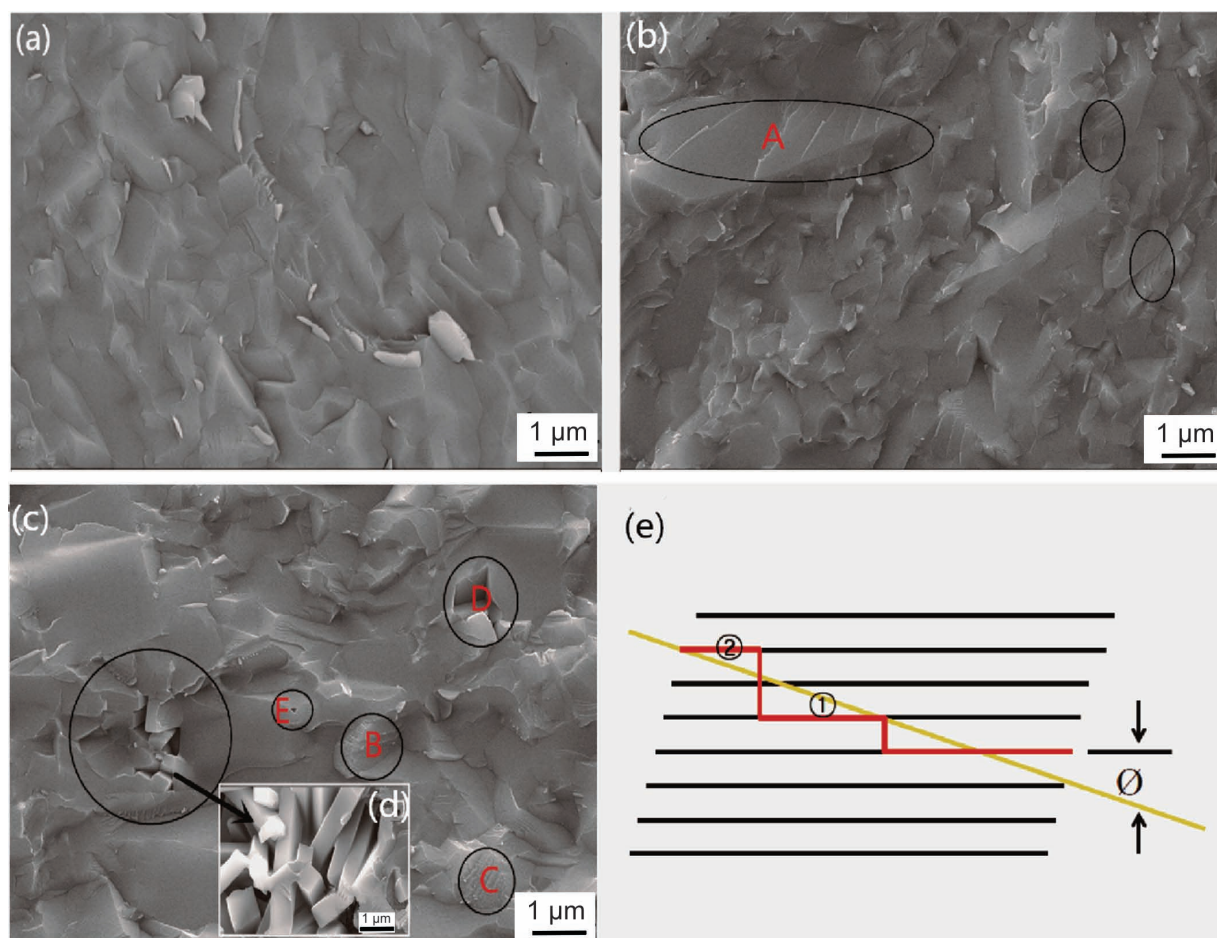
Fig. 4: Fracture surface of ZrO_2-added mullite: (a) fracture surface of pure mullite; (b) fracture surface of 2# specimen showing cleavage steps; (c) fracture surface of 3# specimen showing sharp-edged pores and surface marking; (d) higher magnification showing grains; and (e) a schematic illustration of the fracture mode.

contorted grain boundaries at grain boundaries and grain boundary junctions is found to favor cleavage, with the pores and contorted grain boundaries acting as stress concentrators. As neighboring grains may have slightly different orientations, the cleavage crack changes direction at a grain boundary to continue propagation on the preferred cleavage plane. Within a grain, a crack may grow simultaneously on two parallel crystallographic planes. The two parallel cracks join along the line where they overlap, either by secondary cleavage or by shear to form a step. A number of cleavage steps may join and form a multiple step; cleavage steps of opposite sign may join and disappear. Merging of cleavage steps results in a 'river pattern', so called because of its resemblance to a river and its tributaries [20]. Hence, high flexural strength values in the ZrO_2-added sample (~ 289 ± 12 MPa, Fig. 6) must be related to the formation of cleavage steps. Step formation restraints the propagation of brittle cracks by absorbing extra energy in the vicinity of the connecting stress-riser between adjacent crack planes.

The polished and etched micrographs (from 0 wt% ZrO_2, 2.0 wt% ZrO_2 and 4.0 wt% ZrO_2) are shown in Figs. 5(a) – 5(c). The Vickers indentation marking with cracking on the tips for fracture toughness measurement is shown in Fig. 5(b). Fig. 5(d) shows the morphology of the fracture surface of 4.0 wt% ZrO_2. The relation between the indent size and the microstructure are adequate

to apply the indentation method. The average microhardness for the samples is shown in Fig. 3. It shows that the microhardness of zirconia composites obtained a notable increase and then decreased with further additions. Intergranular cracks through the mullite and the mullite matrix are also observed in Fig. 5(a) and Fig. 5(b), respectively. The dark grain is mullite and the bright grain is zirconia, which is shown in Figs. 5(c) – 5(d), the zirconia grains have been embedded within a mullite matrix. Some close micro-pores are found in Fig. 5(d), and no cleavages can be observed. The formation of close pores can impede the sample's densification, and have a negative effect on flexural strength (see Fig. 6(b)).

As shown in Fig. 6(a), XRD patterns are obtained from the surface of pure mullite and 4.0 wt% ZrO_2-toughened mullite samples to analyze the phase composition. Only tetragonal phase is detected in the ZrO_2-toughened mullite samples, and the tetragonal phase is metastable. Owing to the lower surface energy of the tetragonal phase compared with monoclinic one, metastable tetragonal ZrO_2 can exist at room temperature [22]. It has been reported that conversion of tetragonal zirconia to monoclinic zirconia is noticeably inhibited by the presence of silica (SiO_2) and the silica stabilizes zirconia in tetragonal phase [23].
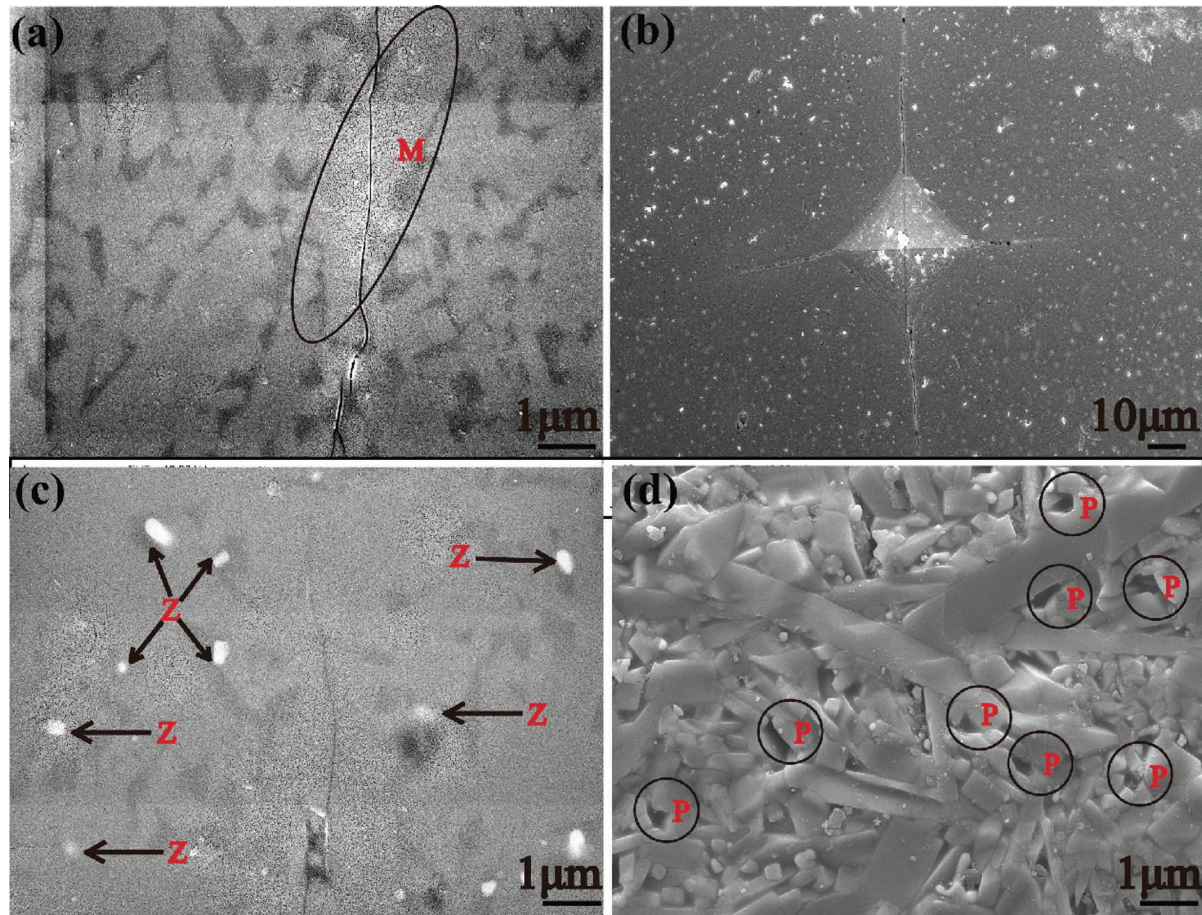
Fig. 5: SEM images: (a) polished surface of 0#; (b) the Vickers indentation of 2#; (c) polished surface of 4#; and (d) fracture surface of 4#.

(4)   Mechanical properties

The flexural strength and fracture toughness are shown in Fig. 6(b). The flexural strength first increased from 179 ± 2.6 MPa to 289 ± 12 MPa with a small amount of ZrO_2 (2.0 wt%) added, and then decreased with a further increase in the content of ZrO_2. The fracture mode was changed from intergranular fracture to transgranular fracture when ZrO_2 was introduced, which could be observed in Figs. 4(a) – 4(c) and Fig. 5(d). When the transgranular fracture occurred, it was able to absorb much more fracture energy. The flexural strength of the composite was almost doubled compared with that of pure mullite. With the increase in additions, cavities and intracrystalline pores were formed which acted as stress concentrators, could store much more fracture energy and were the highest point of fracture energy[24]. These points were the most vulnerable places in the whole sample, so the specimens could be easily broken when subjected to a small external force.

However, the value for fracture toughness (~ 1.38 MPa·√m) does not represent a notable increase in this approach. The t-m transformation involves a positive change of volume, it is appealing to consider that the compressive stress has a negative effect on crack expansion and it can enhance fracture toughness. When no transformation occurred, the enhancement effect was weakened. That is why the values for fracture toughness have not changed significantly.
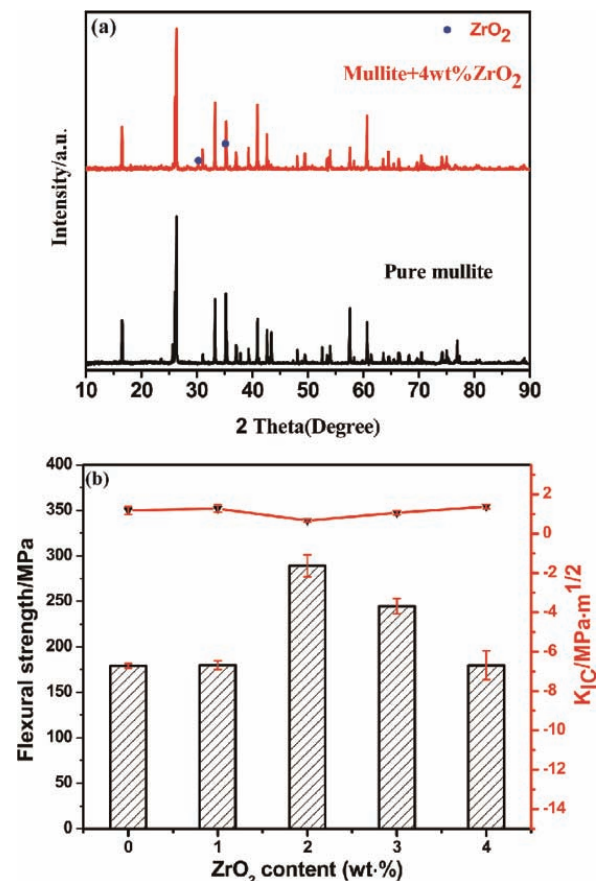

Fig. 6: (a) XRD patterns; (b) the flexural strength and fracture toughness of ZrO_2-added mullite.

IV. Conclusions

The precursor powders were fabricated using the co-precipitation method. The dense samples obtained had more than 97 % of the theoretical density under the sintering conditions of 1500 °C for 7 min with the SPS method. The flexural strength value increased from 179 ± 2.6 MPa to 289 ± 12 MPa and the value for Vickers hardness increased from 7.17 GPa to 9.99 GPa with a small amount of ZrO_2 (2.0 wt%) added, respectively. However, the value for fracture toughness did not exhibit any notable increase. Extensive fine cleavage was observed on the grain surface. A number of cleavage steps may join and form a multiple step, high flexural strength values must be related to the formation of cleavage steps.

Acknowledgments

References

[1] Rendtorff, N.M., Sárez,, G., Sakka, Y., Agliettia, E.F.: Dense mullite zirconia composites obtained from the reaction sintering of milled stoichiometric alumina zircon mixtures by SPS, *Ceram. Int.*, **40**, 4461 – 4470, (2014).

[2] Khor, K.A., Yu, L.G., Li, Y., Dong, Z.L., Munir, Z.A.: Spark plasma reaction sintering of ZrO_2/mullite composites from plasma spheroidized zircon/alumina powders, *J. Mater. Sci. Eng. A*, **339**, 286 – 296, (2003).

[3] Kong, L.B., Zhang, T.S., Ma, J., Boey, F., Zhang, R.F.: Mullite phase formation in oxide mixtures in the presence of Y_2O_3, La_2O_3 and CeO_2, *J. Alloy. Compd.*, **372**, 290 – 299, (2004).

[4] Schneider, H., Schreuer, J., Hildmann, B.: Structure and properties of mullite: A review, *J. Eur. Ceram. Soc.*, **28**, 329 – 344, (2008).

[5] Ashrafi, H., Emadi, R., Zamani Foroushani, R.: Synthesis and characterization of mullite-zirconia nanostructured composite by combined mechanical activation and reaction sintering, *Adv. Powder Technol.*, **26**, 1452 – 1457, (2015).

[6] Cameron, W.E.: Mullite: A substituted alumina, *Am. Mineral.*, **62**, 747 – 755, (1977).

[7] Angel, R.J., Prewitt, C.T.: Crystal-structure of mullite: A re-examination of the average structure, *Am. Mineral.*, **71**, 1476 – 1482, (1986).

[8] Amutharani, D., Gnanam, F.D.: Low temperature pressureless sintering of sol-gel derived mullite, *Mater. Sci. Eng. A*, **264**, 254 – 261, (1999).

[9] Zhang, G., Wang, Y., Fu, Z., Wang, H., Wang, W., Zhang, J., Lee, S.W., Niihara, K.: Transparent mullite ceramic from single-phase gel by spark plasma sintering, *J. Eur. Ceram. Soc.*, **29**, 2705 – 2711, (2009).

[10] Kong, L.B., Zhang, T.S., Ma, J., Boey, F., Zhang, R.F.: Mullite phase formation in oxide mixtures in the presence of Y_2O_3, La_2O_3 and CeO_2, *J. Alloy. Compd.*, **372**, 290 – 299, (2004).

[11] Hong, S.H., Cermignani, W., Messing, G.L.: Anisotropic grain growth in seeded and B_2O_3-doped diphasic mullite gels, *J. Eur. Ceram. Soc.*, **16**, 133 – 141, (1996).

[12] Dong, Y., Hampshire, S., Zhou, J., Ji, Z., Wang, J., Meng, G.: Sintering and characterization of flyash-based mullite with MgO addition, *J. Eur. Ceram. Soc.*, **31**, 687 – 695, (2011).

[13] Souto, P.M., Menezes, R.R., Kiminami, R.H.G.A.: Effect of Y_2O_3 additive on conventional and microwave sintering of mullite, *Ceram. Int.*, **37**, 241 – 248, (2011).

[14] Sedmale, G., Steins, I., Zalite, I., Mezinskis, G.: Microstructure and properties of mullite-ZrO_2 ceramics with silicon nitride additive prepared by spark plasma sintering, *Ceram. Int.*, **42**, 3745 – 3750, (2016).

[15] Omori, M.: Sintering, consolidation, reaction and crystal growth by the spark plasma system (SPS), *J. Mater. Sci. Eng. A*, **287**, 183 – 188, (2000).

[16] Rendtorff, N.M., Gómez, S., Gauna, M.R., Conconi, M.S., Suarez, G., Aglietti, E.F.: Dense mullite-zirconia-zirconium titanate ceramic composites by reaction sintering, *Ceram. Int.*, **42**, 1563 – 1572, (2016).

[17] Munir, Z.A., Anselmi-Tamburini, U.: The effect of electric field and pressure on the synthesis and consolidation of materials: A review of the spark plasma sintering method, *J. Mater. Sci.*, **41**, 763 – 777, (2006).

[18] Ghahremani, D., Ebadzadeh, T., Maghsodipour, A.: Spark plasma sintering of mullite: relation between microstructure, properties and spark plasma sintering (SPS) parameters, *Ceram. Int.*, **41**, 6409 – 6416, (2015).

[19] Carvalho, R.S., Oliveira, F.J., Silva, R.F., Costa, F.M.: Mechanical behaviour of zirconia-mullite directionally solidified eutectics, *Mater. Design*, **6**, 211 – 216, (2014).

[20] Doni Jayaseelan, D., Amutha Rani, D., Benny Anburaj, D., Ohji, T.: Pulse electric current sintering and microstructure of industrial mullite in the presence of sintering aids, *Ceram. Int.*, **30**, 539 – 543, (2004).

[21] Lawn, B.: Fracture of brittle solids, Cambridge University Press, 1993.

[22] Garvie, R.C., Hanninck, R.H., Pascoe, R.T.: Ceramic steel? *Nature* (London), **258**, 703 – 704, (1975).

[23] Yugeswaran, S., Selvarajan, V., Tok, A.I.Y., Siva Rama Krishna, D.: Twin step synthesis of mullite and mullite-zirconia composite in low power transferred arc plasma (TAP) torch, *Mater. Charact.*, **62**, 419 – 424, (2011).

[24] Torrecillas, R., Calderon, J.M., Moya, J.S., Reece, M.J., Davies, C.K.L., Olagnon, C., Fantozzi, G., Suitability of mullite for high temperature applications, *J. Eur. Ceram. Soc.*, **19**, 2519 – 2527, (1999).